Picosecond to Hour Time Scale Dynamics of a "Three Finger" Toxin: Correlation with Its Toxic and Antigenic Properties†

Marc Guenneugues, Pascal Drevet, Suzanne Pinkasfeld, Bernard Gilquin, André Ménez, and Sophie Zinn-Justin*

Département d'Ingénierie et d'Etudes des Protéines, CEA, Saclay, 91191 Gif-sur-Yvette Cedex, France

Received May 30, 1997; Revised Manuscript Received August 28, 1997⊗

ABSTRACT: Toxin α from *Naja nigricollis* (61 amino acids, four disulfide bridges) belongs to the "three finger" fold family, which contains snake toxins with various biological activities and nontoxic proteins from different origins. In this paper, we report an extensive ^{1}H and ^{15}N NMR study of the dynamics of toxin α in solution. ^{15}N relaxation, ^{1}H off-resonance ROESY, and H−D exchange experiments allowed us to probe picosecond to hour motions in the protein. Analysis of these NMR measurements demonstrates that toxin α exhibits various time scale motions, i.e., particularly large amplitude picosecond to nanosecond motions at the tips of the loops, observable microsecond to millisecond motions around two disulfide bridges, second time scale motions around the C−N bonds of asparagine and glutamine side chains which are more or less rapid depending on their amino acid solvent accessibility, and minute to hour motions in the *β*-sheet structure. The less well-defined regions of toxin α solution structures are subject to important picosecond to nanosecond motions. The toxic site is organized around residues belonging to the rigid core of the molecule but also comprises residues exhibiting dynamics on various time scales. The Mα1 epitope is subject to large picosecond to millisecond motions, which are probably modified by the interaction with the antibody. This phenomenon could be linked to the neutralizing properties of the antibody.

Toxin α from *Naja nigricollis* is an α-neurotoxin containing 61 amino acids and four disulfide bridges (Eaker & Porath, 1967). Its three-dimensional structure has been determined on the basis of proton NMR[1] data (Zinn-Justin et al., 1992): toxin α folds into three major loops stabilized by four disulfide bridges (Figure 1). It belongs to the "three finger" fold family containing snake toxins with a variety of biological activities: α-neurotoxins are antagonists of the nicotinic acetylcholine receptor and block neuromuscular transmission (Endo & Tamiya, 1991); cardiotoxins act at the membrane level by changing the permeability and/or by directly affecting the membrane organization (Dufton & Hider, 1991); fasciculins are inhibitors of synaptic acetylcholinesterases (Rodriguez-Ithurralde et al., 1983); mambin is an antagonist of platelet aggregation and of cell−cell adhesion (McDowell et al., 1992). The three finger fold is also adopted by nontoxic proteins from other origins: CD59 is an inhibitor of complement system activation (Sugita et al., 1988); domains of the urokinase-type plasminogen activator (Ploug & Ellis, 1994) and xenoxins from the skin secretion of *Xenopus laevis* (Kolbe et al., 1993) are also probably folded according to the three finger motif. While three-dimensional structures of a large number of these proteins have been determined [see review by Albrand et al. (1995)], their movements in solution have been essentially characterized on a minute to hour time scale by NMR hydrogen exchange kinetic measurements. In the case of α-neurotoxins, such experiments have suggested that the amplitude of structural fluctuations is linked to the reversibility of the neuromuscular block, thus emphasizing the importance of internal dynamics in the toxic activity (Miyazawa et al., 1983).

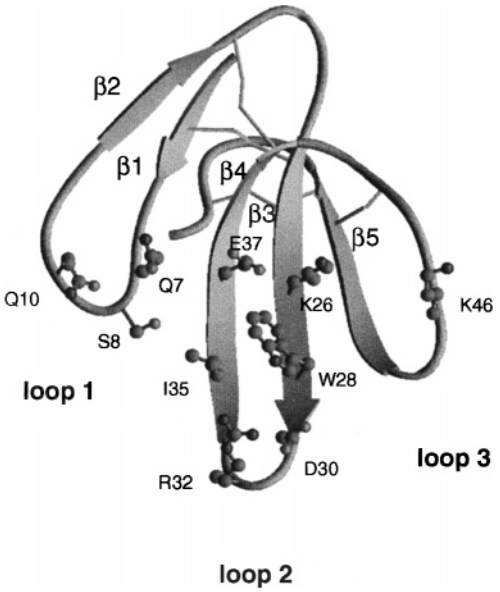

FIGURE 1: Schematic representation of the solution structure of toxin α (Zinn-Justin et al., 1992). The backbone (in ribbon), the 4 disulfide bridges (in sticks), and the 10 side chains critical for the protein biological activity (in ball and sticks) are displayed. The toxin backbone folds into a double-stranded *β*-sheet formed by *β*1- (E2 to H4) and *β*2- (T14 to T16) strands and a triple-stranded *β*-sheet formed by *β*3- (C23 to R29), *β*4- (T34 to C40), and *β*5- (I49 to C54) strands. The representation of toxin α was generated using the Ribbons package (Carson, 1987).

Localization of the nicotinic acetylcholine receptor binding site of the α-neurotoxin erabutoxin *a* from *Laticauda semifasciata* has been probed by mutagenesis analysis (Pillet et al., 1993; Trémeau et al., 1995). Ten residues are involved

† M.G. was financially supported by IFSBM (Villejuif, France).

* To whom correspondence should be addressed.

⊗ Abstract published in *Advance ACS Abstracts,* December 1, 1997.

[1] Abbreviations: NMR, nuclear magnetic resonance; HSQC, heteronuclear single-quantum correlation; TOCSY, total correlation spectroscopy; NOE, nuclear Overhauser effect; NOESY, nuclear Overhauser effect spectroscopy; ROESY, rotating frame Overhauser effect spectroscopy; rmsd, root-mean-square deviation.

S0006-2960(97)01293-2 CCC: $14.00

in the binding of erabutoxin *a* to its target. Six of them are highly conserved in α-neurotoxins and are thought to constitute a "common functional core" through which α-neurotoxins establish conservative contacts with the receptor. All ten residues are present in toxin α, suggesting that the active site of toxin α is similar to that of erabutoxin *a*. These ten residues are essentially located in loop 2, three of them are situated at the extremity of loop 1 and one at the extremity of loop 3 (Figure 1). The poor definition of the tips of loops 2 and 3 in the NMR solution structures of toxin α (Zinn-Justin et al., 1992) suggests that the proposed active site is highly mobile. Constructing molecules presenting the biological activity of toxin α has been undertaken on the basis of the protein three-dimensional structure (Cuniasse et al., 1995; Zinn-Justin et al., 1996). As protein folding, stability, and biological activity are linked to protein dynamics, design of new antagonists of nicotinic acetylcholine receptor should take into account not only the structure but also the motions of toxin α in solution.

The epitopes corresponding to two antibodies neutralizing toxin α have been identified by NMR and mutagenesis analysis (Zinn-Justin et al., 1993; Ducancel et al., 1996). One of these antibodies, called Mα1, has been shown to accelerate the dissociation of toxin−receptor complex (Boulain & Ménez, 1982). It has been proposed that binding of Mα1 in the upper part of loop 1 induces a conformational change in the toxic site, i.e., the lower part of loops 1, 2, and 3 (Boulain & Ménez, 1982). However, nothing is known about the mobility of the epitope or about correlated motions between the upper part of loop 1 and the toxic site.

In this paper, we report the characterization of the backbone dynamics of toxin α on a time scale ranging from picoseconds to hours. The questions we want to address are the following: (i) Is the poor resolution of some regions of the solution structures of toxin α due to mobility? (ii) Does the active site exhibit some motions? (iii) Does the Mα1 epitope exhibit some motions? (iv) What is the time scale of the motions we may reveal in the different regions of the protein?

MATERIALS AND METHODS

Preparation of NMR Samples. The ^{15}N-labeled sample of toxin α was obtained as described (Drevet et al., 1996). ^{15}N-Labeled protein (14 mg) was dissolved in 400 μL of 90% H_2O/10% D_2O, so that the final concentration was 5 mM. Microliter amounts of HCl were added to adjust the pH of the sample to 3.5. The sample of native toxin α consisted of a 400 μL solution of 5 mM protein in 90% H_2O/10% D_2O at pH 3.5.

^{15}N Relaxation Experiments. All ^{15}N relaxation experiments were carried out at 308 K on a Bruker AMX or DRX 500 MHz spectrometer. ^{15}N resonances (Figure 2) were assigned on the basis of the ^{1}H assignment (Zinn-Justin et al., 1992) by analyzing HSQC (Bodenhausen & Ruben, 1980), HSQC-TOCSY (Otting & Wüthrich, 1988), and HSQC-NOESY (Bax et al., 1990; Norwood et al., 1990) experiments. ^{15}N R_1 measurements were carried out using the pulse sequence published by Kay et al. (1992) with relaxation delays of 20, 50, 100, 200, 500, 1000, and 1500 ms. Off-resonance ^{15}N $R_{1\rho}$ measurements were carried out as described in Zinn-Justin et al. (1997). Radio frequency (RF) field powers ω_1 ranging from 1.2 to 2.2 kHz were

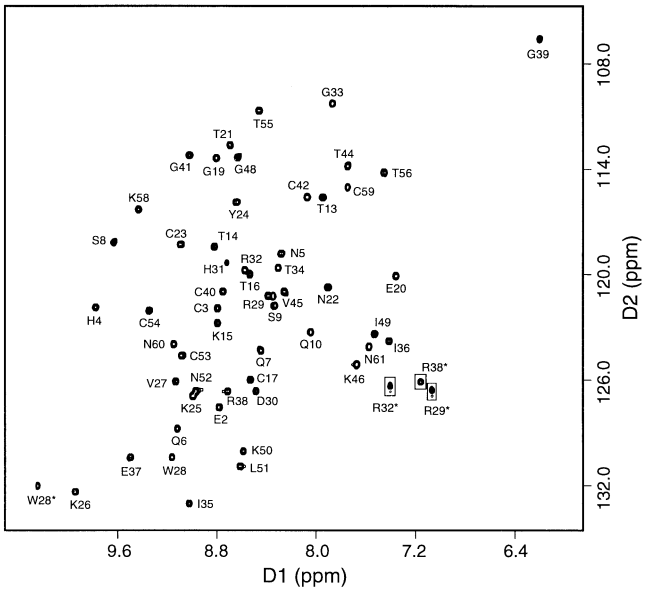

FIGURE 2: Contour plot of a ^{15}N−^{1}H experiment recorded using the R_1 measurement pulse sequence of Kay et al. (1992) and a relaxation time of 30 ms. The three boxed antiphase peaks are folded back in F_1 and correspond to arginine side-chain ($N_\epsilon H_\epsilon$) correlations.

applied during the relaxation time; the offset of the RF irradiation was adjusted so that the nitrogen magnetization was locked on an axis making an effective θ angle of 35°, 45°, or 55° with the B_0 axis. In order to calculate each $R_{1\rho}(\theta, \omega_1)$ parameter, seven experiments with relaxation delays of 30, 60, 150, 300, 500, 800, and 1200 ms were recorded. The NOE measurements were carried out using the pulse sequence published by Kay et al. (1992). Amide proton saturation during the NOE period was achieved using GARP decoupling (Shaka et al., 1983) for 4 s, i.e., approximately eight times the T_1 of the longest backbone amide ^{15}N nucleus, to ensure generation of the steady-state NOE. In all of these experiments, the water signal was suppressed using a WATERGATE sequence (Piotto et al., 1992). Quadrature detection in the indirect dimension was obtained using the States−TPPI phase cycling scheme (Marion et al., 1989). The matrix size was 1024 × 256 data points using 32 scans per increment.

All data sets were Fourier-transformed after application of a 90° shifted sine-bell apodization window and zero-filling in both dimensions to yield a matrix of 1024 × 1024 real points, using FELIX 95.0 software (MSI/Biosym, San Diego, CA). Peak heights were measured on each 2D spectrum using FELIX macros written by Mikael Akke. R_1 values were obtained by a three-parameter exponential least-squares fit. $R_{1\rho}(\theta, \omega_1)$ values were obtained by a two- or three-parameter exponential least-squares fit, depending on the phase cycling used (Sklenar et al., 1987). $R_{1\rho}(\theta, \omega_1)$ is related to R_1, R_2, and R_{ex} according to (Zinn-Justin et al., 1997)

$$R_{1\rho}(\theta, \omega_1) = \cos^2 \Theta\, R_1 + \sin^2 \Theta\, R_2 + R_{ex}(\Theta, \omega_1)$$

where R_2 is the transverse self-relaxation rate for the fast motion contribution (correlation time inferior to 1 μs; prevailing mechanisms, dipole−dipole and CSA interactions) and $R_{ex}(\Theta, \omega_1)$ is the relaxation rate associated to the slow motion processes (chemical exchange contribution). $R_{1\rho}$ values were taken as the average $\langle R_{1\rho}(90°, \omega_1/\sin \Theta)\rangle$

computed from the two offset $R_{1\rho}(\theta, \omega_1)$ data set (Zinn-Justin et al., 1997). The $^1H \rightarrow {}^{15}N$ NOE were calculated as

$$\eta = (I_{sat}/I_{unsat})$$

where I_{sat} and I_{unsat} are the peak heights in the spectra recorded with and without proton saturation, respectively. The errors on R_1, $R_{1\rho}$, and NOE values were estimated by calculating the standard error of two, six, and two separate data sets, respectively.

R_1, $R_{1\rho}$, and NOE parameters were analyzed using the Modelfree 3.1 program developed by A. Palmer (1991). This treatment implies an isotropic model of the molecule where the global and internal motions are not correlated. The spectral density can then be written as

$$J(\omega) = (2/5)[S^2\tau_c/(1 + \omega^2\tau_c^2) + (1 - S^2)\tau/(1 + \omega^2\tau^2)]$$

τ_c being the global isotropic correlation time, τ_e the effective internal correlation time [$\tau = (1/\tau_c + 1/\tau_e)^{-1}$], and S^2 the generalized order parameter. On the basis of the expressions of R_1, $R_{1\rho}$, and NOE as a function of $J(\omega)$, we extracted S^2, τ_e, and an R_{ex} exchange term for each NH vector. The errors made on S^2, τ_e, and R_{ex} were calculated on the basis of the errors estimated on R_1, $R_{1\rho}$, and NOE and 500 Monte-Carlo simulations of the fit to these three values.

The influence of anisotropy on the S^2 and τ_e parameters has been shown not to be significant in the case of the amino-terminal fragment of urokinase-type activator (Hansen et al., 1994) and of human ubiquitin (Tjandra et al., 1995). However, when anisotropy is not recognized, residues with a high $R_{1\rho}/R_1$ ratio may be misinterpreted as being subject to conformational exchange (Shurr et al., 1994; Tjandra et al., 1996). Therefore, we checked the influence of toxin α anisotropy on our Modelfree results. We computed the diffusion tensor of toxin α using HYDRO software (Garcia de la Torre et al., 1981) that calculates the hydrodynamic properties of macromolecules represented by a bead model (Bloomfield et al., 1967). The hydrodynamic calculations were performed on the toxin α minimized averaged NMR structure (Zinn-Justin et al., 1992), hydrated by placing the protein in a large box of water, energy minimizing, and keeping all water oxygens within 3.7 Å of the protein. Protein heavy atom and water oxygen atom radii *a* were assigned to 1.0 and 1.6 Å, respectively. Friction constants $\zeta = 4\pi\eta a$ were used, where η is the viscosity (Venable et al., 1988). Tjandra et al. (1995) presented a method which allows derivation of the diffusion tensor from experimental R_1 and $R_{1\rho}$ values. However, in toxin α, of the 24 NH which satisfy the selection criteria of Barbato et al. (1992), only two have an orientation which deviates by less than 60° from the highest component principal axis of the diffusion tensor calculated with HYDRO. When sampling of the NH vector orientations relative to the principal axes of the diffusion tensor is poor, the approach developed by Tjandra et al. (1995) is inefficient. We therefore used the hydrodynamic modeling results for the asymmetry and anisotropy coefficients characterizing the shape of toxin α and for the average rotational diffusion tensor *D* (i.e., one-third of the trace of the diffusion tensor) calibrated to $1/\tau_c$. The S^2, τ_e, and R_{ex} parameters were fitted to the experimental R_1, $R_{1\rho}$, and NOE data using the spectral density function corresponding to an asymmetric molecule (Woessner, 1962; Lipari & Szabo, 1982; Tjandra et al., 1995).

Another approach was used in order to characterize fast chemical exchange without making any assumption on the motion model. It is based on the analysis of the off-resonance $R_{1\rho}(\theta, \omega_1)$ dependence upon the applied ω_1 RF field, as described in Zinn-Justin et al. (1997).

Off-Resonance ROESY Experiments. Off-resonance ROESY experiments (Desvaux et al., 1993, 1995) were carried out at 308 K in a Bruker 500 MHz spectrometer. We used a pulse sequence with adiabatic rotations (Desvaux et al., 1995) and irradiation at two offsets to minimize the angular dispersion (Desvaux & Goldman, 1996). Mixing times of 20, 40, and 60 ms were used at 9.7°, 19.3°, 43.4°, and 52.6° in order to construct a buildup curve at each angle. To filter for pure exchange effects, an experiment was also recorded using a mixing time of 50 ms and an angle of 35.3°. The various angles were obtained by applying a 10 kHz spin−lock RF field at different offset values. The water signal was suppressed using a WATERGATE sequence as in the ^{15}N relaxation experiments. Quadrature detection in the indirect dimension was obtained using the TPPI phase cycling scheme (Marion & Wüthrich, 1983). The matrix size was 4096 × 256 data points using 64 scans per increment.

All data sets were Fourier-transformed after application of a 90° shifted squared sine-bell apodization window in both dimensions and zero-filling to yield 2048 × 1024 real point matrices. Volumes were measured using the integration facility provided in the Xwin-nmr 1.0 software (Bruker Analytische Messtechnik GmbH, Rheinstetten, Germany).

The effective dipolar cross-relaxation rates [$\sigma_{ij}^{eff}(\theta)$] were taken as proportional to the slope of the straight line fitted to the build-up curves comprising the cross-peak volumes at the various mixing times and the point (0; 0). They can be expressed as (Desvaux et al., 1993)

$$\sigma_{ij}^{eff}(\theta) = \sigma_{ij} \cos^2\theta + \mu_{ij} \sin^2\theta$$

A Marquardt fitting (Press et al., 1992) of this equation gave us the longitudinal (σ_{ij}) and the transversal (μ_{ij}) dipolar cross-relaxation rate for each studied proton pair (*i*,*j*).

The ratio $F_{ij} = \sigma_{ij}/\mu_{ij}$ is independent of the interproton distance and reflects the fluctuations of the interatomic vector $\mathbf{r}_{ij}$. Figure 3 displays the variations of F_{ij} as a function of the order parameter S^2 and of the internal correlation time τ_e at 500 MHz and with a τ_c of 3.7 ns (i.e., the overall rotational correlation time calculated for toxin α; see Results), assuming that the radial and angular fluctuations of the interproton vector are uncorrelated. It shows that, with the stated assumptions, and for this τ_c value, the F_{ij} ratio is poorly sensitive to low-amplitude fluctuations ($F_{ij} > -0.4$ implies $S^2 < 0.5$) so that high values of this ratio should indicate the presence of important picosecond to nanosecond fluctuations of the $\mathbf{r}_{ij}$ vector.

However, when polarization transfer occurs between exchanging protons, the apparent relaxation rates are modified as follows:

$$\sigma_{ij} = (\sigma_{ij})_{dipolar} + k_{ij}$$

$$\mu_{ij} = (\mu_{ij})_{dipolar} + k_{ij}$$

where k_{ij} is the exchange rate between protons *i* and *j*. The effective relaxation rate measured becomes then

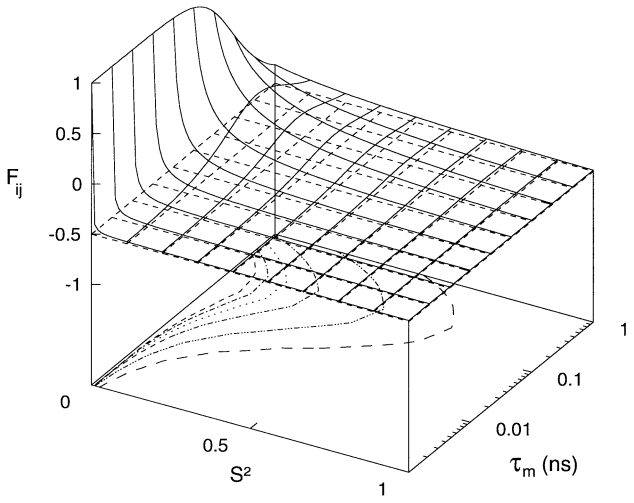

FIGURE 3: 3D plot of the ratio $F_{ij} = \sigma_{ij}/\mu_{ij}$ as a function of the order parameter S^2 and the internal correlation time τ. The 3D plot (in solid lines) was generated assuming the spectral density model (2) and an overall rotational correlation time of 3.7 ns. The plane corresponding to the theoretical minimum value of F_{ij} (−0.5) is represented by regularly dashed lines. Curves drawn in the (S^2, τ) plane are projections of the F_{ij} envelope at particular values (- - -, 0; -·-, −0.1; ···, −0.2; -···-, −0.3; -····-, −0.4; − − −, −0.45).

$$\sigma_{ij}^{\text{eff}}(\theta) = (\sigma_{ij}^{\text{eff}}(\theta))_{\text{dipolar}} + k_{ij}$$

In this case, the F_{ij} ratio is lowered; it can even become positive if $k_{ij} > (\mu_{ij})_{\text{dipolar}}$.

Analysis of the F_{ij} ratio seems to be a good criterion to evidence proton pairs subject to fast internal dynamics of high amplitude ($F_{ij} > -0.5$) or subject to a slow exchange phenomenon ($F_{ij} < -0.5$ or $F_{ij} > 0.0$).

Proton−Deuterium Exchange Experiments. Proton−deuterium exchange experiments were carried out at three temperatures, 283, 298, and 318 K, in a Bruker AMX 600 MHz spectrometer. The exchanges were studied on the sample of native toxin α lyophilized from H_2O and redissolved in pure D_2O. The exchange kinetics of the amide protons were followed by recording absolute value COSY experiments over 48 h. Each experiment comprised 256 FIDs of four scans composed of 1024 time−domain data points and lasted 15 min. Data processing was performed using NMRi software (New Methods Research Inc., New York). Exchange rates were determined by least-squares fitting a single-exponential decay to the volumes of non-overlapping H_N-H_α COSY cross-peaks.

RESULTS

Overall Rotational Motion of Toxin α. The ^{15}N relaxation experiments give information on the picosecond to nanosecond motions of the NH vectors. The ^{15}N R_1, ^{15}N $R_{1\rho}$, and $^1H \rightarrow {}^{15}N$ NOE parameters were measured on toxin α. Complete quantitative data were obtained for 52 of the 55 backbone amides. The good dispersion of the cross-peaks in the $^{15}N-{}^1H$ fingerprint region is shown in Figure 2. The remaining three backbone amides did not yield quantitative data because of a lack of ^{15}N assignment (D57) or a partial overlap between two peaks (T16, R32).

R_1, $R_{1\rho}$, and NOE values are reported in Table 1 and plotted as a function of the residue number in Figure 4. Standard errors in the ^{15}N relaxation parameters were obtained from a set of independent measurements (Table 1). For 83% (i.e., 43/52) of the amides, the errors in R_1 are lower than 5%, and for 98% (i.e., 51/52), they are lower than 7%. Similar results were found for the $R_{1\rho}$ and NOE parameters: 73% (i.e., 38/52) of the amides exhibit errors in $R_{1\rho}$ lower than 5% and 96% (i.e., 50/52) lower than 7%. With the NOE, 85% (i.e., 44/52) of the amides exhibited errors lower than 5% and 100% lower than 7%. These errors were used as uncertainties in the Monte Carlo simulation part of the Modelfree analysis.

A first estimation of the overall rotational correlation time of toxin α was derived from the 2.10 ± 0.18 average value of the $R_{1\rho}/R_1$ ratio calculated for the 24 residues satisfying NOE > 0.65 and $(\langle T_{1\rho}\rangle - T_{1\rho,n})/\langle T_{1\rho}\rangle - (\langle T_1\rangle - T_{1,n})/\langle T_1\rangle >$ 1.5 SD, where $T_{x,n}$ is the T_x value of residue n, $\langle T_x\rangle$ is the average T_x value, and SD is the standard deviation of $(\langle T_{1\rho}\rangle - T_{1\rho,n})/\langle T_{1\rho}\rangle - (\langle T_1\rangle - T_{1,n})/\langle T_1\rangle$ (Barbato et al., 1992). It corresponds to an isotropic overall rotational correlation time τ_c value of 3.8 ± 0.4 ns. Such a τ_c value is consistent with those found for other proteins of similar molecular weight, such as human type α transforming growth factor (50 residues, $\tau_c = 3.8$ ns at 303 K; Li et al., 1995), B1 domain (56 residues, $\tau_c = 3.3$ ns at 299 K; Barchi et al., 1994), eglin *c* (70 residues, $\tau_c = 4.2$ ns at 309 K; Peng & Wagner, 1992), or calbindin D_{9k} (75 residues, $\tau_c = 4.3$ ns at 300 K; Kördel et al., 1992).

Hydrodynamic modeling gave a τ_c of 3.6 ns, an anisotropy $D_z/(D_x + D_y)$ value of 1.35, and an asymmetry D_x/D_y value of 1.06. The calculated τ_c value falls in the interval deduced from the average $R_{1\rho}/R_1$ ratio, which makes us confident in the anisotropy and asymmetry values found by HYDRO.

The Lipari−Szabo parameters characterizing the movements of each backbone NH vector, i.e., the order parameter S^2, the effective internal correlation time τ_e, and an exchange term R_{ex}, were extracted from the ^{15}N relaxation data using Modelfree 3.1 software which assumes an isotropic model. τ_e and R_{ex} were found to be significant (i.e., greater than their errors) and were optimized for 44 and 23 residues, respectively. The overall rotational correlation time τ_c was optimized during this procedure and converged to a value of 3.7 ns.

These parameters were also calculated assuming an anisotropic model. Not surprisingly, as only 6 of the 52 studied residues have an NH vector orientation that deviates by less than 60° from the highest component principal axis of the rotational diffusion tensor, and the asymmetry is 1.06, no significant differences were found between the results of the isotropic and anisotropic calculations for the S^2 and τ_e values. R_{ex} values were generally lowered by the use of an anisotropic model but remain in the error interval, except for T21, C41, T56, and N60. For T21, R_{ex} decreases from 4.45 to 4 Hz and remains significant. In contrast, the R_{ex} value of C41 decreases from 0.65 to 0.3 Hz, and that of T56 and N60 drops from about 0.4 Hz to 0. The observed sensitivity of the R_{ex} value in the chosen model emphasizes the interest of using methods that directly probe conformational exchange.

In order to discuss results independent of the chosen model for the overall global motion, we present in this paper data obtained with an isotropic model, but taking into account only R_{ex} values derived from the Modelfree analysis when they are sufficiently high (higher than 1 Hz) or when they are shown to depend on the RF field power.

Table 1: Experimental ^{15}N Relaxation Data and Optimized Modelfree Parameters[a]

residue	R_1 (Hz)	$R_{1\rho}$ (Hz)	$R_{1\rho}/R_1$	NOE	S^2	τ_e (ps)	R_{ex} (Hz)
2	2.55 ± 0.07	5.96 ± 0.16	**2.34 ± 0.13**	0.65 ± 0.02	0.830 ± 0.024	31.04 ± 15.2	0.809 ± 0.232
3	2.54 ± 0.03	6.68 ± 0.22	**2.63 ± 0.11**	0.66 ± 0.01	0.818 ± 0.008	24.41 ± 6.28	1.551 ± 0.223
4	2.68 ± 0.00	5.42 ± 0.19	**2.03 ± 0.07**	0.66 ± 0.03	0.863 ± 0.006	36.19 ± 23.22	
5	2.74 ± 0.13	6.69 ± 0.26	**2.44 ± 0.22**	0.69 ± 0.03	0.893 ± 0.044		1.117 ± 0.380
6	3.03 ± 0.15	5.25 ± 0.17	**1.73 ± 0.14**	0.68 ± 0.03	0.872 ± 0.025	23.57 ± 24.1	
7	2.65 ± 0.03	5.24 ± 0.20	1.98 ± 0.10	0.63 ± 0.04	0.847 ± 0.012	49.96 ± 27.23	
8	2.64 ± 0.04	5.91 ± 0.24	2.24 ± 0.12	0.59 ± 0.03	0.837 ± 0.014	75.84 ± 21.62	0.620 ± 0.246
9	2.33 ± 0.05	6.25 ± 0.21	2.68 ± 0.14	0.64 ± 0.01	0.748 ± 0.015	24.84 ± 4.95	1.545 ± 0.231
10	2.59 ± 0.18	5.48 ± 0.28	**2.12 ± 0.25**	0.65 ± 0.03	0.859 ± 0.036	36.52 ± 32.97	
13	2.55 ± 0.05	5.25 ± 0.08	**2.06 ± 0.07**	0.70 ± 0.02	0.837 ± 0.010		
14	2.56 ± 0.02	5.94 ± 0.19	**2.32 ± 0.09**	0.67 ± 0.02	0.828 ± 0.008	16.6 ± 11.08	0.752 ± 0.195
15	2.59 ± 0.18	5.57 ± 0.27	2.15 ± 0.26	0.62 ± 0.03	0.865 ± 0.036	68.54 ± 73.17	
17	2.36 ± 0.14	10.06 ± 0.35	4.26 ± 0.39	0.67 ± 0.01	0.765 ± 0.044	10.5 ± 6.47	5.273 ± 0.437
19	2.23 ± 0.14	4.81 ± 0.24	2.16 ± 0.25	0.56 ± 0.02	0.736 ± 0.029	54.32 ± 12.03	
20	2.29 ± 0.06	6.38 ± 0.22	2.79 ± 0.17	0.64 ± 0.04	0.735 ± 0.021	20.15 ± 12.54	1.767 ± 0.251
21	2.36 ± 0.06	9.22 ± 0.15	3.91 ± 0.16	0.65 ± 0.03	0.760 ± 0.018	18.58 ± 11.29	4.458 ± 0.190
22	2.45 ± 0.07	4.95 ± 0.10	**2.02 ± 0.10**	0.65 ± 0.02	0.790 ± 0.013	21.9 ± 9.42	
23	2.55 ± 0.08	6.11 ± 0.20	2.39 ± 0.15	0.62 ± 0.02	0.816 ± 0.025	48.87 ± 14.1	0.974 ± 0.256
24	2.75 ± 0.01	5.40 ± 0.23	**1.96 ± 0.09**	0.66 ± 0.02	0.887 ± 0.004	41.64 ± 15.94	
25	2.79 ± 0.12	5.44 ± 0.23	**1.95 ± 0.16**	0.68 ± 0.02	0.886 ± 0.025	24.54 ± 19.79	
26	2.66 ± 0.00	5.00 ± 0.27	1.88 ± 0.10	0.64 ± 0.02	0.854 ± 0.005	49.38 ± 17	
27	2.53 ± 0.09	5.61 ± 0.40	2.21 ± 0.24	0.61 ± 0.02	0.809 ± 0.028	48.96 ± 15.07	0.515 ± 0.400
28	2.67 ± 0.15	5.32 ± 0.25	**1.99 ± 0.21**	0.67 ± 0.02	0.856 ± 0.030	21.72 ± 13.59	
29	2.32 ± 0.05	5.55 ± 0.12	**2.40 ± 0.10**	0.67 ± 0.03	0.755 ± 0.017	0.847 ± 0.151	
30	2.26 ± 0.00	4.72 ± 0.20	2.08 ± 0.09	0.57 ± 0.02	0.716 ± 0.014	43.35 ± 17.82	
31	2.47 ± 0.15	4.65 ± 0.46	1.88 ± 0.30	0.44 ± 0.03	0.745 ± 0.039	115.9 ± 47.38	
33	2.05 ± 0.14	4.22 ± 0.14	2.05 ± 0.21	0.46 ± 0.00	0.651 ± 0.02	64.42 ± 5.86	
34	2.06 ± 0.10	4.67 ± 0.09	2.26 ± 0.16	0.54 ± 0.02	0.647 ± 0.032	39.62 ± 7.49	0.557 ± 0.222
35	2.47 ± 0.04	5.22 ± 0.18	2.11 ± 0.11	0.61 ± 0.03	0.789 ± 0.014	43.95 ± 16.08	0.248 ± 0.172
36	2.64 ± 0.07	5.42 ± 0.35	**2.06 ± 0.19**	0.65 ± 0.02	0.851 ± 0.021	36.61 ± 15.09	
37	2.57 ± 0.05	5.04 ± 0.29	**1.96 ± 0.15**	0.66 ± 0.03	0.827 ± 0.016	26.1 ± 15.19	
38	2.62 ± 0.03	5.08 ± 0.23	**1.94 ± 0.11**	0.66 ± 0.02	0.841 ± 0.010	30.08 ± 14.98	
39	2.58 ± 0.16	5.46 ± 0.34	**2.11 ± 0.26**	0.68 ± 0.02	0.858 ± 0.04		
40	2.47 ± 0.00	5.34 ± 0.15	**2.16 ± 0.07**	0.71 ± 0.04	0.804 ± 0.002	0.328 ± 0.148	
41	2.60 ± 0.07	5.940 ± 0.34	**2.29 ± 0.19**	0.69 ± 0.04	0.847 ± 0.022	0.658 ± 0.348	
42	2.48 ± 0.00	4.75 ± 0.12	**1.92 ± 0.05**	0.65 ± 0.00	0.798 ± 0.002	23.21 ± 1.04	
44	2.24 ± 0.10	4.75 ± 0.29	2.12 ± 0.22	0.59 ± 0.00	0.724 ± 0.026	37.71 ± 5.93	
45	2.51 ± 0.26	4.66 ± 0.30	1.86 ± 0.31	0.50 ± 0.00	0.729 ± 0.019	75.73 ± 19.13	
46	2.21 ± 0.06	4.56 ± 0.27	2.06 ± 0.17	0.45 ± 0.00	0.682 ± 0.015	78.02 ± 6.03	
48	2.25 ± 0.04	5.21 ± 0.16	2.32 ± 0.11	0.50 ± 0.03	0.698 ± 0.013	64.76 ± 9.2	0.750 ± 0.172
49	2.29 ± 0.02	5.28 ± 0.17	2.31 ± 0.09	0.63 ± 0.00	0.734 ± 0.007	23.92 ± 2.7	0.672 ± 0.168
50	2.53 ± 0.00	5.84 ± 0.40	2.31 ± 0.17	0.57 ± 0.02	0.799 ± 0.004	71.75 ± 9.22	0.776 ± 0.392
51	2.43 ± 0.00	4.95 ± 0.30	2.03 ± 0.13	0.59 ± 0.00	0.772 ± 0.002	51.82 ± 4.17	
52	2.77 ± 0.12	5.15 ± 0.24	1.86 ± 0.17	0.64 ± 0.01	0.854 ± 0.024	49.32 ± 26.98	
53	2.44 ± 0.04	5.24 ± 0.21	2.15 ± 0.12	0.59 ± 0.02	0.776 ± 0.01	50.98 ± 8.05	0.341 ± 0.207
54	2.77 ± 0.07	5.25 ± 0.20	**1.89 ± 0.12**	0.65 ± 0.02	0.876 ± 0.020	45.33 ± 20.69	
55	2.43 ± 0.01	5.06 ± 0.10	**2.08 ± 0.05**	0.67 ± 0.02	0.785 ± 0.005	14.72 ± 9.01	0.144 ± 0.098
56	2.62 ± 0.03	5.53 ± 0.12	2.11 ± 0.07	0.59 ± 0.01	0.831 ± 0.011	74.53 ± 10.54	0.274 ± 0.134
58	2.64 ± 0.04	5.29 ± 0.12	2.00 ± 0.08	0.63 ± 0.03	0.845 ± 0.012	50.47 ± 20.8	
59	2.80 ± 0.12	5.46 ± 0.21	**1.95 ± 0.16**	0.68 ± 0.04	0.893 ± 0.026		
60	2.79 ± 0.01	6.02 ± 0.23	**2.16 ± 0.09**	0.70 ± 0.00	0.907 ± 0.003	0.367 ± 0.211	
61	2.49 ± 0.06	4.63 ± 0.29	1.86 ± 0.16	0.56 ± 0.03	0.778 ± 0.018	68.15 ± 15.47	
mean	2.52 ± 0.20	5.52 ± 0.99	2.10 ± 0.21	0.62 ± 0.06			
W28	2.10 ± 0.11	4.24 ± 0.38		0.55 ± 0.02	0.66 ± 0.03	38.49 ± 7.34	
R29	0.42 ± 0.10	0.18 ± 0.50		−1.60 ± 0.02	0.06 ± 0.01	44 ± 2	
R32	0.71 ± 0.10	0.95 ± 0.25		−0.66 ± 0.02	0.16 ± 0.01	49 ± 3	
R38	2.30 ± 0.23	4.25 ± 0.27		0.57 ± 0.01	0.70 ± 0.03	41 ± 7	

[a] Reported are the mean value and the standard deviation for backbone (upper part) and side-chain (lower part) nitrogens. [b] The mean value of the $R_{1\rho}/R_1$ ratio was computed on backbone nitrogens which satisfy the criteria of Barbato et al. (1992); the ratio of these nitrogens is displayed in boldface numbers.

Backbone Motions on the Picosecond to Nanosecond Time Scale. The variation of S^2 as a function of the sequence is displayed in Figure 5a. As S^2 is well-defined all along the sequence (errors in the S^2 values are always lower than 6%), significant variations can be observed. Sixty percent (31/52) of the amides have S^2 values greater than or equal to 0.8. Eleven of the 13 studied amides of loop 1, and in particular the five studied amides of the double-stranded β-sheet, also have high S^2 values (Figure 5b). Fourteen of the 20 amides of the triple-stranded β-sheet of loops 2 and 3 also have S^2 values greater than or equal to 0.8: this β-sheet is essentially rigid on the picosecond to nanosecond time scale. Forty percent (21/52) of the amides have S^2 values between 0.65 and 0.8. They are essentially located in or 1 or 2 positions next to a β-turn. Two of them, corresponding to L51 and C53, are located in the β5-strand of loop 3 but are not involved in the hydrogen-bonding network of the triple β-sheet. The last amide corresponds to the C-terminal

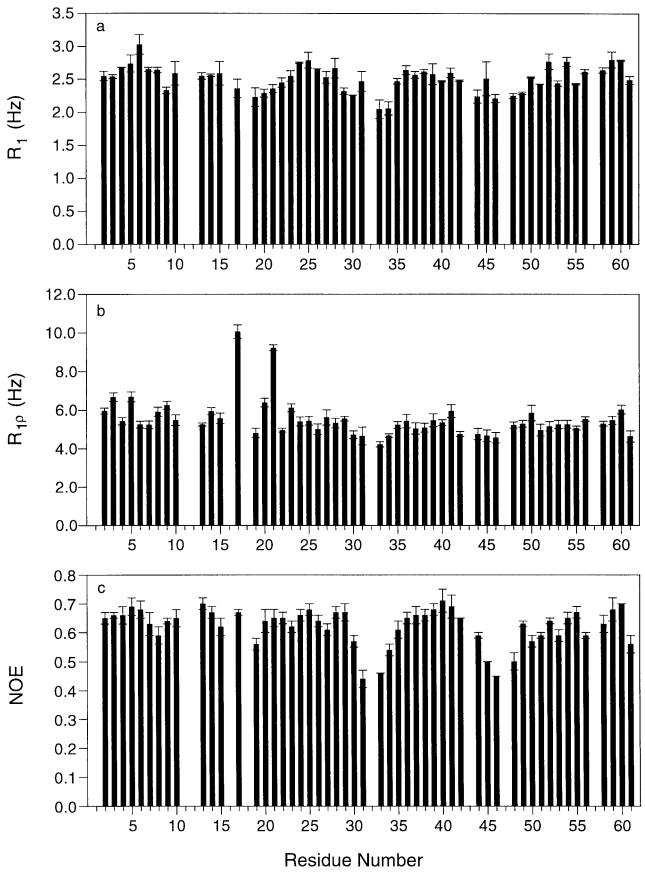

FIGURE 4: (a) R_1, (b) $R_{1\rho}$, and (c) NOE values (in hertz) of the backbone nitrogens of toxin α at pH 3.5 and 308 K. Plotted values and error bars are the average and standard error of two (R_1), 6 ($R_{1\rho}$), and two (NOE) data sets, respectively.

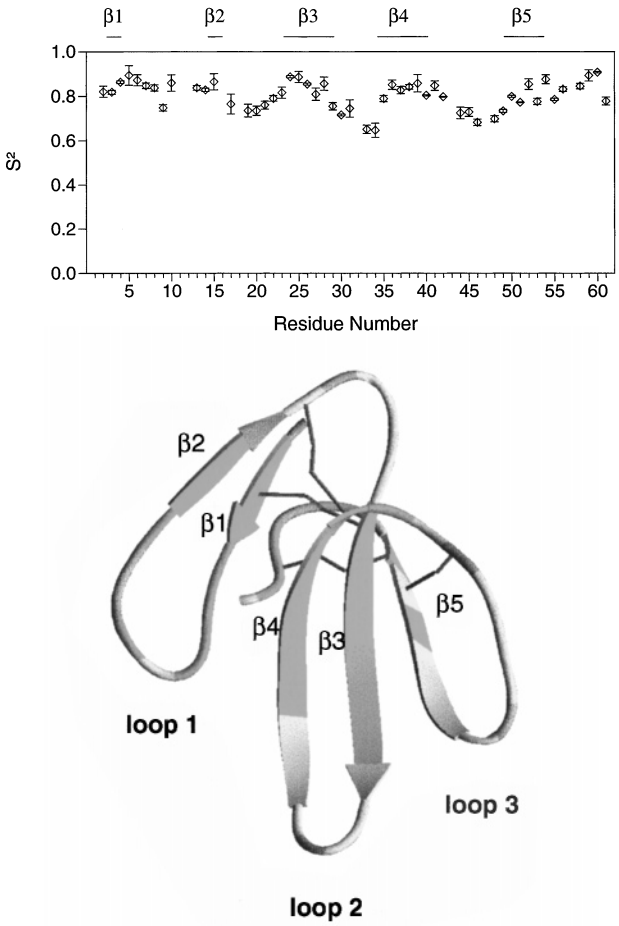

FIGURE 5: Order parameters S^2 calculated by Modelfree 3.1 (Palmer, 1991). (a, top) Order parameters S^2 are plotted as a function of the sequence; the error bars represent the uncertainties derived from a Monte Carlo simulation (500 tries using the errors estimated in R_1, $R_{1\rho}$, and NOE values). (b, bottom) Order parameter S^2 ranges are displayed on a ribbon representation of the structure of toxin α; residues with an S^2 value greater/less than 0.8 are colored in red/yellow; gray indicates residues for which no information is available.

residue. Thus, the secondary structure appears to be an important determinant of the picosecond to nanosecond backbone motions in toxin α. This has already been observed in several, but not all, NMR relaxation studies (Stone et al., 1992; Buck et al., 1995). In other respects, residues whose side chains are buried and which form the protein core [H4, Y24, K26, R38, N60, and the eight cysteines; see Zinn-Justin et al. (1992)] have NH order parameters greater than 0.76. Thus, the side-chain/side-chain interactions seem to be a critical damping factor of the picosecond to nanosecond motions, as described for other proteins [see, for example, Buck et al. (1995)].

Estimations of τ_e are much less precise than estimations of S^2. All the τ_e values are found between 0 and 120 ps, and the errors in τ_e may reach 100%. However, high τ_e values are essentially found in the β-turn of loops 1 and 2 (S8, D31, G33), in loop 3 (V45, K46, G48, K50), and in the C-terminal β-turn (T56). Such values are consistent with the low S^2 values found in these regions, where large amplitude motions occur on the picosecond to nanosecond time scale.

Side-Chain Motions on the Picosecond to Nanosecond Time Scale. S^2 and τ_e parameters were also obtained for the side-chain NH vectors of tryptophan W28 and arginines R29, R32, and R38.

The order parameter of the side-chain NH of the tryptophan is 0.66 ± 0.03, and its correlation time is 38.5 ± 7.5 ps. These values are very similar to that obtained for the backbone NH of the tip of loop 2, i.e., for the most mobile backbone NH of toxin α, suggesting the presence of relatively important picosecond to nanosecond motions at the center of the hydrophobic cluster of the active site. In a motional model where the internal motion corresponds to a free diffusion in a cone of a semiangle α (Lipari & Szabo, 1982), the order parameter is related to α according to

$$S^2 = [\cos(\alpha)(1 + \cos(\alpha))/2]^2$$

and an S^2 value of 0.66 corresponds to an α semiangle of 30°.

However, the arginines show larger picosecond to nanosecond motion amplitudes. If R38 has S^2 and τ_e values close to those of W28 ($S^2 = 0.70 \pm 0.03$ and $\tau_e = 41 \pm 7$ ps), R29 and R32 have a much lower S^2 [S^2(R29) = 0.06 ± 0.01; S^2(R32) = 0.16 ± 0.01] but similar τ_e [τ_e(R29) = 44 ± 2 ps; τ_e(R32) = 49 ± 3 ps]. The motions of the NH_ϵ vectors of R29 and R32 are particularly poorly spatially restricted; in the free diffusion in a cone model, the corresponding cone semiangle values are 69° and 58°, respectively.

Interestingly, the S^2 values of these side chains are well correlated with their average relative solvent accessibilities computed over an NMR ensemble of structures. W28 and R38, which are found on the central part of loop 2 but on opposite sides of the β-sheet, have S^2 values of 0.66 and

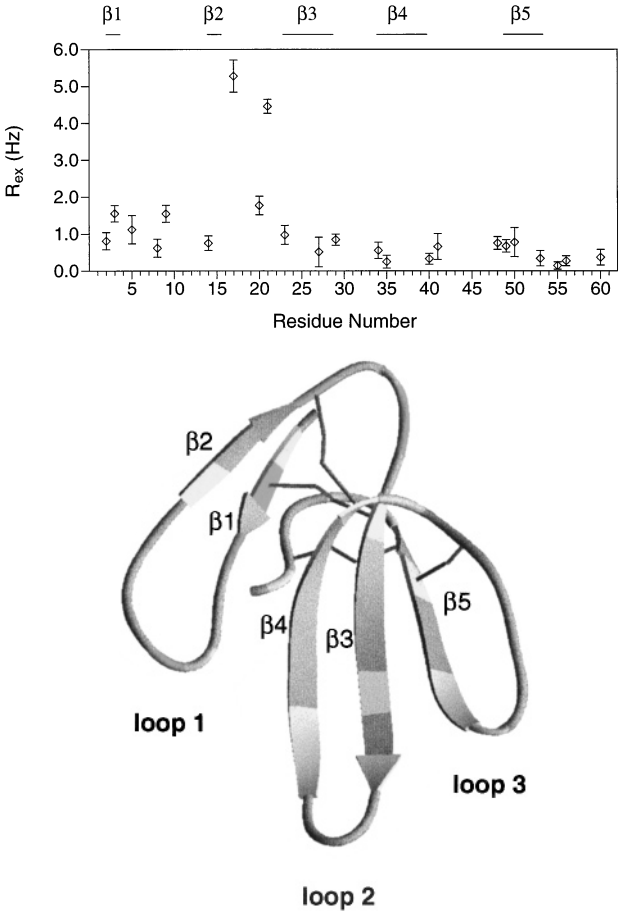

FIGURE 6: Representations of R_{ex} variations in toxin α. (a, top) Exchange terms R_{ex} (in hertz) are plotted as a function of the sequence; error bars were calculated as for the order parameters. (b, bottom) Exchange term R_{ex} ranges are displayed on a ribbon representation of the structure of toxin α; residues with an R_{ex} value greater/less than 1 Hz are colored in red/yellow; gray indicates residues for which no significant R_{ex} value was calculated or no information is available.

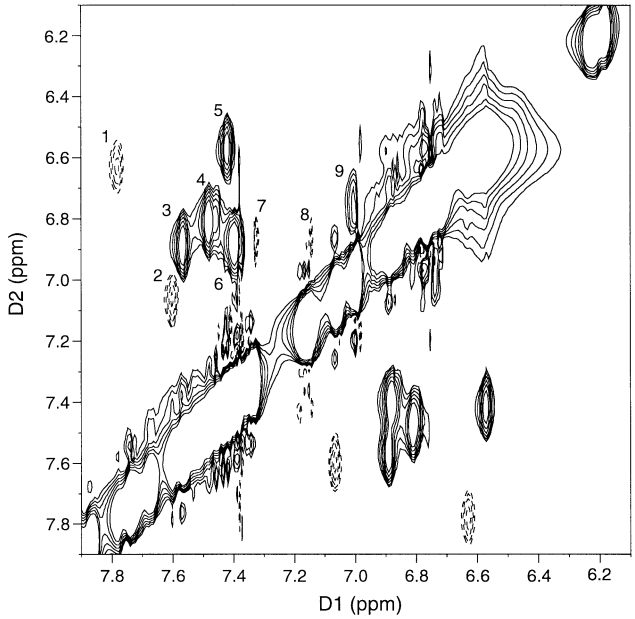

FIGURE 7: Contour plot of an off-resonance ROESY spectrum region showing the cross-relaxation peaks between the NH_2 proton pairs of the asparagine and glutamine side chains. The experiment was recorded with a spin−lock angle of 54.7° and a mixing time of 60 ms. Solid/dashed lines are used to plot positive/negative contours, respectively. Labeled cross-peaks correspond to Q6−$H_{\epsilon 21}$/$H_{\epsilon 22}$ (1), N5−$H_{\delta 21}$/$H_{\delta 22}$ (2), Q10−$H_{\epsilon 21}$/$H_{\epsilon 22}$ (3), N52−$H_{\delta 21}$/$H_{\delta 22}$ (4), N61−$H_{\delta 21}$/$H_{\delta 22}$ (5), Q7−$H_{\epsilon 21}$/$H_{\epsilon 22}$ (6), W28−$H_{\zeta 2}$/$H_{\zeta 3}$ (7), W28−$H_{\eta 2}$/$H_{\zeta 3}$ (8), and N22−$H_{\delta 21}$/$H_{\delta 22}$ (9).

0.70, respectively, and relative solvent accessibilities of 33% and 18%, respectively. R29 and R32, which are found in or next to the β-turn of the tip of loop 2, have S^2 values of 0.06 and 0.15, respectively, and relative solvent accessibilities of 76% and 83%, respectively. A similar correlation has been observed by Buck et al. (1995) for the side chains of lysozyme.

Backbone Motions on the Microsecond to Millisecond Time Scale. Four amides show $R_{1\rho}$ values greater than the mean value (5.52 Hz) plus the standard deviation (0.99 Hz) (Figure 4b). They are located in or next to the β1-strand of loop 1 (C3, N5) and in or next to the β-turn connecting loop 1 to loop 2 (C17, T21), suggesting the presence of microsecond to millisecond motions in these regions of the molecule. The R_{ex} values extracted from the $R_{1\rho}$ parameters through the Modelfree analysis are displayed as a function of the sequence in Figure 6a. The region of toxin α exhibiting the most important exchange phenomena is the turn connecting loop 1 to loop 2 (Figure 6b). In this part of the molecule, C17 and T21 show R_{ex} values greater than 4 s^{-1}. The corresponding exchange time scale was determined by analyzing the dependence of the off-resonance $R_{1\rho}$ value on the effective RF field amplitude; it ranges between 20 and 200 μs (Zinn-Justin et al., 1997). Four other NH vectors show R_{ex} values greater than 1 s^{-1} (Figure 6a): C3 and N5, which are in or next to the β1-strand (loop 1), exhibit an exchange on a 20−200 μs and 1−50 μs time scale, respectively; S9, which is in the loop 1 β-turn, exhibits an exchange on a 1−50 μs time scale; and E20, which is in the turn connecting loop 1 to loop 2, exhibits an exchange on a 20−200 μs time scale (Zinn-Justin et al., 1997). Thus, important motions on the microsecond to millisecond time scale involve disulfide bridges C3−C23 and C17−C40 (even though the 0.3 s^{-1} R_{ex} value for C40 is poorly significant), residues sequentially close to these disulfide bridges (N5, E20, T21), and S9 at the tip of loop 1. Loops 2 and 3 as the C-terminal β-turn appear to be more rigid on this time scale (Figure 6b). In particular, the two disulfide bridges located in this region of the molecule exhibit no observable exchange phenomena.

Side-Chain Motions on the Second Time Scale. The only nonscalar cross-peaks observable in the 35.3° experiment concern correlations between H_δ or H_ϵ of asparagines or glutamines, respectively. A region of the spectrum corresponding to the experiment recorded with an angle of 54.7° and a 60 ms mixing time is displayed in Figure 7. It shows that some of the correlations between H_δ or H_ϵ of asparagines or glutamines still give rise to positive cross-peaks at this high angle value. They are the only protons subject to a measurable exchange phenomenon on the millisecond to second time scale. For slower exchange rates, the polarization transfer is too low to induce measurable cross-peaks, while for larger exchange rates, one observes a single line at an average frequency.

The $F_{ij} = (\sigma_{ij}/\mu_{ij})$ ratio was calculated for a data set of 244 correlations between expected nonexchanging proton pairs (no cross-peak observed on the 35.3° experiment), giving rise to significant intensities (signal to noise ratio > 5), and with a chemical shift difference greater than 0.5 ppm

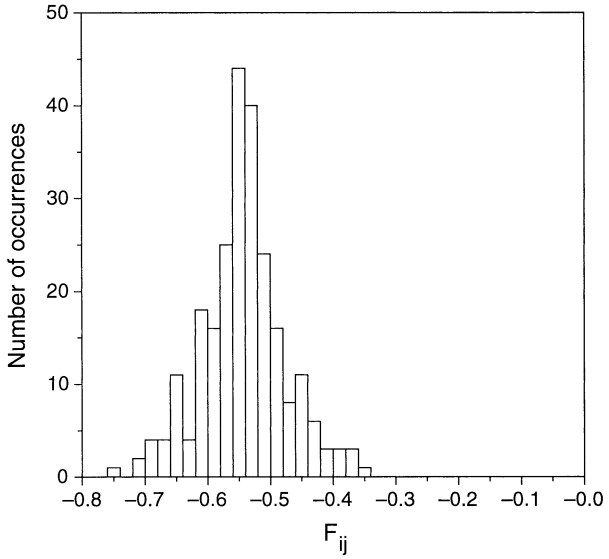

FIGURE 8: Histogram of the distribution of the $F_{ij} = \sigma_{ij}/\mu_{ij}$ ratios calculated for a set of 244 correlations between expected nonexchanging proton pairs. The data set is composed of 57 backbone/backbone, 123 backbone/side-chain and 64 side-chain/side-chain correlations; it comprises 132 intraresidual, 75 sequential, and 37 long-range correlations.

in order to eliminate a bias due to the diagonal proximity. These ratios exhibit a Gaussian distribution centered at −0.54 with a half-width of 0.06 (Figure 8). The center of the distribution is lower than −0.5, the theoretical lower limit of the F_{ij} ratio. This must be due to an underestimation of μ_{ij} resulting from a higher relaxation rate in the plane than along the static field ($R_{1\rho} > R_1$). The half-width is in agreement with the estimated errors in σ and μ via a Monte Carlo simulation. Moreover, extracted subsets according to the type of proton pairs exhibiting the dipolar correlation (intraresidual, long-range, backbone/backbone, backbone/side chain, side chain/side chain) exhibit a similar shape. Thus, considering the precision of our data, the ratio F_{ij} appears to be insensitive to the internal dynamics of the interproton $\mathbf{r}_{ij}$ vectors in toxin α. As a first approximation, the dipolar relaxation rates in toxin α can be linked by $(\sigma/\mu)_{\text{dipolar}} = -0.5$, apart from experimental uncertainties.

We have estimated the exchange rates between the H_δ or H_ϵ protons of asparagines and glutamines by two approaches: (1) Assuming $(\sigma_{ij}/\mu_{ij})_{\text{dipolar}} = -0.5$, we extracted $k_{ij}I_0$ from σ_{ij} and μ_{ij} and used an estimation of I_0 obtained by the analysis of isolated diagonal peaks. (2) Assuming the dipolar relaxation is negligible in the 35.3° experiment, we took the cross-peak intensity as $k_{ij}I_0\tau_m$, τ_m being the mixing time.

Both approaches give similar results (Table 2). The observed exchange rates characterize the polarization transfer due to the rotation around the $C_\gamma-N_\delta$ or $C_\delta-N_\epsilon$ bond of the asparagine and glutamine side chains, respectively. The rotation rate of this bond in toxin α then occurs with a time constant close to a second. Interestingly, the measured rotation rates are highly correlated with the side-chain solvent accessibilities. Q7, Q10, and N52 (10 s^{-1}) have a relative accessibility between 51% and 74%; N22 (6 s^{-1}) has a relative accessibility of 34%; N5, Q6, and N60 (<6 s^{-1}) have a relative accessibility between 0 and 31%. Only N61 shows a restricted mobility (6 s^{-1}) when compared to its accessibility (70%).

Table 2: Exchange Rates k_{ex} between H_δ or H_ϵ Protons of Asparagines or Glutamines Obtained with Off-Resonance ROESY Experiments[a]

residue	$k_{ex(1)}$ (Hz)	$k_{ex(2)}$ (Hz)	side-chain solvent accessibility (%)
N5	1.00	0.625	26
Q6	0.79	0.594	31
Q7	12.0	9.27	51
Q10	8.74	6.99	66
N22	5.14	3.19	34
N52	10.30	8.92	74
N60	1.48	0.00	0
N61	6.81	6.00	70

[a] Estimation 1 was extracted from the apparent dipolar relaxation rates measured at various angles assuming that $(\sigma_{ij}/\mu_{ij})_{\text{dipolar}} = -0.5$. Estimation 2 relies on the measurement of the cross-peak intensities in the 35.3° experiment, assuming no dipolar relaxation occurs at this particular angle. The average side-chain solvent accessibilities were computed on the NMR solution structures of toxin α (Zinn-Justin et al., 1992) with the X-PLOR program (Brünger, 1988).

Backbone Motions on Time Scales Greater than the Millisecond. H−D exchange kinetics measurements were previously performed at pH 3.5 and 25 °C (Zinn-Justin et al., 1992) and 10 °C (Zinn-Justin et al., 1993), and new experiments at 45 °C have been recorded. The results show that 27 amide protons have an exchange rate slower than 1 h^{-1} at 25 °C (Figure 9a). They essentially belong to residues defining the secondary structure elements of toxin α. However, they can be separated into two sets when considering their exchange rate at higher temperature.

The first set comprises amide protons exchanging at a rate higher than 1 h^{-1} at 45 °C. These protons are located in loop 1 (E2, C3, N5, and T13 belong or are next to the β-sheet; Q6 belongs to the β-bulge; Q10 belongs to the β-turn), in the β-turn connecting loops 1 and 2 (C17), and in loop 3 (I49 belongs to the β-turn; N52 belongs to the β5-strand).

The second set comprises amide protons exchanging at a rate lower than 1 h^{-1} at 45 °C. These protons belong or are next to the β-sheet of loop 1 (H4, K15), the β-sheet of loop 2 (C23, Y24, K25, K26, V27, W28, I35, I36, E37, R38, G39, G41), the β-strand of loop 3 (C54), and the C-terminal β-turn (T56, K58, N60).

At 45 °C, loops 1 and 3 are more mobile than loop 2 and the C-terminal turn of the molecule (Figure 9b).

DISCUSSION

Rigid Core of the Molecule. Motions of toxin α have been studied on different time scales: from picosecond to nanosecond and from microsecond to millisecond using ^{15}N relaxation measurements, around the second exploiting off-resonance ROESY experiments, and from minutes to hours following H−D exchange kinetics. Interestingly, the central part of loop 1 (H4, K15), the central part of loop 2 (residues Y24 to W28 and I36 to G39), and the C-terminal region (C54, K58) seem to have a rigid backbone on all these time scales: order parameters S^2 are greater than 0.8, no or low R_{ex} exchange terms are measured, and the amide proton signals have a hydrogen exchange rate slower than 1 h^{-1} at 45 °C. Even the side chains of W28 and R38 show a limited flexibility when compared to the other side chains of the molecule: $S^2 = 0.66$ and 0.70, respectively, and $R_{ex} = 0$. In fact, the mobility for all the side chains of H4, Y24 to W28,

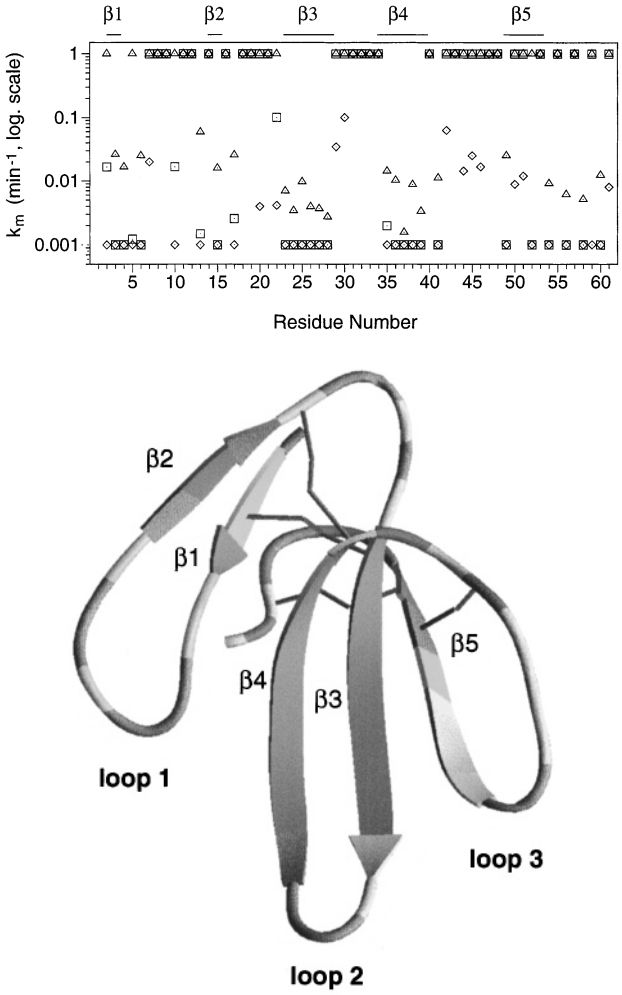

FIGURE 9: H−D exchange rates of toxin α amide protons at pH 3.5 and different temperatures. (a, top) Exchange rates (in min^{-1}) are displayed as a function of the sequence (diamonds, rates measured at 10 °C; squares, 25 °C; triangles, 45 °C). Rates slower than 0.001 min^{-1} are plotted equal to 0.001 min^{-1}, while amide protons that were not observed on the the first COSY experiment recorded to follow the exchange kinetics have an arbitrary exchange rate value of 1 min^{-1}. (b, bottom) Exchange rates are displayed on a ribbon representation of the structure of toxin α; residues whose amide protons have an exchange rate faster than 1 h^{-1} at 45 °C are colored red; remaining residues whose amide protons have an exchange rate faster/slower than 1 h^{-1} at 25 °C are colored orange/yellow; gray indicates residues whose amide proton was not observed on the first COSY experiment.

I36 to G39, C54 and K58 is probably limited as their solvent accessibility is always lower than 60% (Buck et al., 1995). Thus our results suggest that H4, K15, Y24 to W28, I36 to G39, C54, K58 form the rigid core of toxin α and altogether are involved in the stabilization of the three-dimensional structure of the protein.

Motions in the N-Terminal Region L1−C23. Loop 1 (L1−C17) has a more complex behavior: while its backbone is relatively rigid on the picosecond to nanosecond time scale (S^2 are greater than 0.8 for all residues except S9 and C17), and while its structure appears to be relatively stable on a minute to hour time scale (9 of its 17 amides have a hydrogen exchange rate slower than 1 h^{-1} at 25 °C), it is subject to motions on a 1−200 μs time scale. Indeed, four backbone nitrogens of loop 1 show high R_{ex} values; they correspond to C3, N5, S9, and C17 which exhibit a conformational exchange phenomenon on a 20−200, 1−50, 1−50, and 20−200 μs time scale, respectively. The dynamics of the side chains of loop 1 also appear to be contrasted. On the second time scale, the side chains of N5 and Q6 located between the β1-strand and the β-turn exhibit relatively restricted motions, but the side chains of Q7 and Q10 in the β-turn seem to be highly mobile.

The turn connecting loop 1 to loop 2 is highly mobile on all time scales. The backbone from C17 to C21 is subject to important motions on the picosecond to nanosecond time scale ($S^2 < 0.77$). Three nitrogens (C17, E20, and T21) show important R_{ex} values, corresponding to a 20−200 μs time scale conformational exchange phenomenon. And finally, the amide protons of all residues, C17 excepted, have a hydrogen exchange rate faster than 1 h^{-1} at 25 °C.

It should be stressed that if loop 1 seems to be more rigid and more stable than the turn connecting loop 1 to loop 2, the NH vectors submitted to important microsecond to millisecond motions ($R_{ex} > 1$ Hz) are all located in this region.

Where Do Microsecond to Millisecond Motions Come from? It has already been said that, in toxin α, the secondary structure and the side-chain/side-chain interactions are the principal factors influencing the picosecond to nanosecond dynamics. Furthermore, the β-sheet structure is a critical determinant of the amide proton exchange rates. However, the reasons for the distribution of the microsecond to millisecond motions in the L1−C23 region of toxin α are less clear. C3, N5, C17, and E20 amide nitrogens have R_{ex} values greater than 1 Hz and are involved in backbone hydrogen bonds (Zinn-Justin et al., 1992). Molecular dynamics simulations of interleukin 1β (Chandrasekhar et al., 1992) have suggested that the microsecond to millisecond motions involve large amplitude jumps between well-defined conformations stabilized by hydrogen bonds. This could be part of the phenomenon observed in toxin α. Moreover, as nitrogens with high R_{ex} values are all located in the same region of the molecule, the motions of their NH vectors could be correlated. Such a dynamical phenomenon has already been observed in well-defined β-sheet structures and attributed to breathing motions of the β-sheet (Redfield et al., 1992; Cheng et al., 1993). In our case, in between the 10 nitrogens showing significant R_{ex} values in the L1−C23 region, only E2, C3, T14, and C17 nitrogens are found in the β-sheet of loop 1. Thus, the microsecond to millisecond motions of loop 1 probably result from a more complex phenomenon. As most of the toxin nitrogens showing R_{ex} values larger than 1 Hz belong to cysteines or to residues sequentially close to cysteines, a conformational change of the C17−C40 and/or C3−C23 disulfide bridges could be a determining event in the motion process. Szyperski et al. (1993) have already characterized such a phenomenon. They observed a dynamic equilibrium between two conformational states of the C14−C38 disulfide bridge in BPTI. The time scale of this motion was close to the millisecond. The time scale of the motion of the NH(C17) in toxin α is 20−200 μs (Zinn-Justin et al., 1997). It is faster than what has been found for BPTI. However, the effect of the steric environment on the disulfide bridge exchange rate is great (Creighton, 1993). Calculations have shown that a disulfide bridge trans conformation costs about 7−9 kcal/mol (Fraser et al., 1971). This should correspond to a time scale of 10−100 μs (Kopple et al., 1988), which is not very far from Szyperski's observation and consistent with what we found.

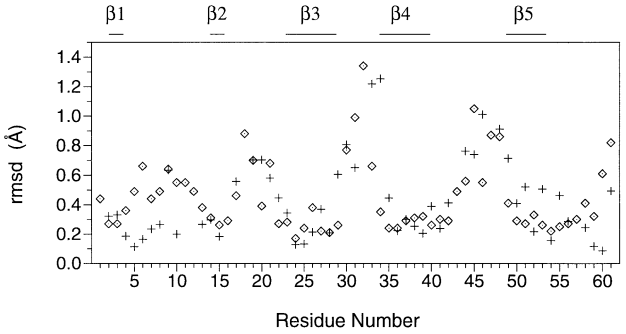

FIGURE 10: Superposition of the average root-mean-square deviation (diamonds) calculated for the Cα atoms of the NMR structures (in angstroms) with an appropriate function of the backbone S^2 (crosses). The empirically defined function applied to the order parameter for this comparison is $10(1 - S^2)^2$.

Correlation between Motions and NMR Solution Structure Resolution. Figure 10 shows the superposition of the average rmsd calculated for the Cα atoms of the NMR structures with an appropriate function applied to the backbone S^2 values. Both curves are strongly correlated to the secondary structure (Zinn-Justin et al., 1992). Furthermore, as found for other proteins (Redfield et al., 1992; Peng et al., 1992; Grasberger et al., 1993; Buck et al., 1995), the variations of the two curves are similar: when going from the highest to the lowest values, one finds for both curves the tip of loop 2, then the region T44−I49 of loop 3, the turn connecting loop 1 to loop 2, the C-terminus, loop 1, and finally the triple-stranded β-sheet structure. However, there is not a strict correlation between both data sets (Figure 10): the maximum value of $(1 - S^2)$ corresponds to T34, and the maximum values of the rmsd correspond to R32 (for which we could not determine the order parameter) and V45; the minimum value of $(1 - S^2)$ corresponds to N60, and the minimum value of the rmsd corresponds to Y24. Particularly large and numerous differences between the two curves are found in loop 1. On the picosecond to nanosecond time scale, most of this loop (E2−S8, Q10, T13−K15) appears to be as rigid as the triple-stranded β-sheet, but the resolution of the NMR solution structures is close to that of the triple-stranded β-sheet only for residues involved in the double-stranded β-sheet (E2−H4, T13−T16). The difficulties that have been encountered to define the conformation of residues N5−S8 and Q10 could be linked to the microsecond to millisecond motions occurring in this region of toxin α, as maybe to slower motions. In the β5-strand (I50−C54), the rmsd values appear to be insensitive to the fact that the amide protons are alternately involved in a β-sheet structure, and thus in stable hydrogen bonds, while the S^2 values clearly show that some picosecond to nanosecond motions are damped when the amide proton is involved in a stable β-sheet hydrogen bond. Thus, if the rmsd variations are globally related to picosecond to nanosecond and, as suggested, slower motions in toxin α, caution should be taken in their interpretation in terms of dynamics. It must be stressed that the rmsd depends on the number and distribution of the interproton distance restraints which are related not only to dynamics but also to proton packing density (Powers et al., 1993). This can add some differences between $(1 - S^2)$ and rmsd variations.

Motions in the Active Site of Toxin α. Ten side chains are critical for the binding of erabutoxin a from *L. semifasciata* to the nicotinic acetylcholine receptor (Trémeau et al., 1995). The sequence of toxin α from *N. nigricollis* is 74% similar to that of erabutoxin *a* and contains in particular these 10 amino acids. We assumed that the active site of toxin α is essentially formed by the side chains of these 10 residues. Thus, the toxin α active site extends over the tip of loop 1 (Q7, S8, Q10), loop 2 (K26, W28, D30, R32, E37), and the tip of loop 3 (K46). It is formed around a set of residues (K26, W28, E37) which belong to the rigid core of the molecule. However, it contains residues from the two most mobile regions of the molecule on the picosecond to nanosecond time scale: D30 and R32 at the tip of loop 2 and K46 at the tip of loop 3. The side chain of R32 is particularly mobile: the motions of its NH_ϵ bond appear to be almost not spatially restricted on the picosecond to nanosecond time scale. It also contains residues Q7, S8, and Q10. They are located at the tip of loop 1, the backbone of which is involved in microsecond to millisecond motions (S8 and particularly S9 backbone nitrogens exhibit an exchange term); the side chains of Q7 and Q10 are mobile on the second time scale. Thus, the active site is subject to important dynamics on various time scales, which may play a critical role when toxin α binds to the nicotinic acetylcholine receptor. This may complicate any attempt to reproduce the active site in a different structural context.

Motions in the Mα1 Epitope. Measurement of H−D exchange rates in the Mα1−toxin complex (Zinn-Justin et al., 1993) has allowed us to obtain a general picture of the epitope by identifying a number of residues of toxin α buried upon its interaction with Mα1. Eight side chains were proposed to constitute the Mα1 epitope. They essentially belong to the upper part of loop 1 (E2, N5, T13, T14, K15, T16, P18); one belongs to the C-terminal region (K58). Dynamics information on the picosecond to nanosecond and microsecond to millisecond time scales is available for six of these eight residues. This information shows that most of the Mα1 epitope is rigid on the picosecond to nanosecond time scale but that it is subject to microsecond to millisecond motions. Indeed, E2, N5, T13, T14, K15, and K58 have backbone S^2 values greater than 0.8; the side chain of N5 is relatively rigid on the second time scale; however, E2, N5, and T14 backbone nitrogens show R_{ex} values larger than 0.75 Hz. For T16 and P18, no data are available on picosecond to millisecond dynamics. However, as C17 and G19 are highly mobile on the picosecond to nanosecond time scale and C17 is subject to important microsecond to millisecond motions, it seems reasonable to suggest that residues T16 and P18 are mobile on the whole picosecond to millisecond time scale as well.

Mα1 has been shown to accelerate the dissociation of the toxin−receptor complex (Boulain & Ménez, 1982). Moreover, the Mα1 epitope is distinct from the presumed toxic site (Zinn-Justin et al., 1993). This argues for the model of Boulain et al. (1982) in which Mα1 binds to the receptor−toxin complex, forming a transient ternary complex which destabilizes the initial receptor−toxin complex. Our study of toxin α dynamics shows that numerous residues of loop 1 are subject to microsecond to millisecond motions. Moreover, among these residues, S9 is located between two residues of the toxic site; C3, N5, T14, and C17 belong or are next to the Mα1 epitope. Thus, assuming the microsecond to millisecond motions in loop 1 are correlated, we may propose that the binding of toxin α to Mα1 or to the receptor favors one or the other of the microsecond to millisecond equilibrium conformational states, respectively.

This hypothesis could be confirmed by studying the structure and dynamics of toxin α bound to the antibody and to the receptor.

Conclusion. ^{15}N relaxation measurements, off-resonance ROESY experiments, and H−D exchange kinetic studies have given us information about toxin α backbone and side-chain dynamics on picosecond to hour time scales, thus enabling us to characterize the motions in the toxic site and in one of the epitopes of the protein.

In toxin α, the central part of loop 2 and the C-terminal region appear to be relatively rigid on the explored time scales, while loop 1 is essentially subject to millisecond to second motions. It has to be stressed that, as this is the first study of the dynamics of a three finger molecule on such a large time scale, no comparison with analogous protein dynamics is possible. However, sequence comparison of three finger toxins presenting different biological activities shows that essentially four residues are conserved in addition to the eight cysteines. These residues are Y24 and G39 in the central part of loop 2, P43 between loop 2 and loop 3, and N60 in the C-terminal region of the molecule. No residues are conserved in loop 1, and the precise position of loop 1 relative to loops 2 and 3 has been difficult to determine for some toxins (Le Du et al., 1992; Zinn-Justin et al., 1994; Albrand et al., 1995). It has even been shown to vary with the solvent and when the toxin binds to its target in the case of fasciculin (Le Du et al., 1996; Bourne et al., 1995). Therefore, the apparent rigidity of the central part of loop 2 and the C-terminal region, and the microsecond to second time scale mobility of loop 1, could be general characteristics of three finger toxins.

ACKNOWLEDGMENT

We thank Martial Piotto and Bruker GmbH for recording part of the off-resonance ROESY experiments. We also thank Dr. Arthur Palmer for providing the Modelfree 3.1 software. We are grateful to Drs. Patrick Berthault and Hervé Desvaux for constant technical assistance and fruitful discussions.

REFERENCES

Albrand, J.-P., Blackledge, M. J., Pascaud, F., Hollecker, M., & Marion, D. (1995) *Biochemistry 34*, 5923−5937.

Barbato, G., Ikura, M., Kay, L. E., Pastor, R. W., & Bax, A. (1992) *Biochemistry 31*, 5269−5278.

Barchi, J. J., Grasberger, B., Gronenborn, A. M., & Clore, G. M. (1994) *Protein Sci. 3*, 15−21.

Bax, A., Ikura, M., Kay, L. E., Torchia, D. A., & Tschudin, R. (1990) *J. Magn. Reson. 86*, 304−318.

Bloomfield, V. A., Dalton, W. O., & Van Holde, K. E. (1967) *Biopolymers 5*, 135−148.

Bodenhausen, G., & Ruben, D. (1980) *Chem. Phys. Lett. 69*, 185−189.

Boulain, J.-C., & Ménez, A. (1982) *Science 217*, 732−733.

Boulain, J.-C., Ménez, A., Couderc, J., Faure, G., Liacopoulos, P., & Fromageot, P. (1982) *Biochemistry 21*, 2910−2915.

Bourne, Y., Taylor, P., & Marchot, P. (1995) *Cell 83*, 503−512.

Brünger, A. T. (1988) *X-PLOR Manual*, The Howard Hughes Medical Institute and Department of Molecular Biophysics and Biochemistry, Yale University, New Haven, CT.

Buck, M., Boyd, J., Redfield, C., MacKenzie, D. A., Jeenes, D. J., Archer, D. B., & Dobson, C. M. (1995) *Biochemistry 34*, 4041−4055.

Carson, M. (1997) *J. Mol. Graphics 5*, 103−106.

Chandrasekhar, I., Clore, G. M., Szabo, A., Gronenborn, A. M., & Brooks, B. R. (1992) *J. Mol. Biol. 226*, 239−250.

Cheng, J.-W., Lepre, C. A., Chambers, S., Fulghum, J. R., Thomson, J. A., & Moore, J. M. (1993) *Biochemistry 32*, 9000−9010.

Creighton, T. E. (1993) *in Proteins: Structure and Molecular Properties*, 2nd ed., W. H. Freeman and Company, New York.

Cuniasse, P., Thomas, A., Smith, J. C., Lam Thanh, H., Léonetti, M., & Ménez, A. (1995) *Biochemistry 34*, 12782−12789.

Desvaux, H., & Goldman, M. (1996) *J. Magn. Reson. B110*, 198−201.

Desvaux, H., Berthault, P., Birlirakis, N., & Goldman, M. (1993) *J. Magn. Reson. A108*, 219−229.

Desvaux, H., Berthault, P., Birlirakis, N., Goldman, M., & Piotto, M. (1995) *J. Magn. Reson. A113*, 47−52.

De Weille, J. R., Schweitz, H., Maes, P., Tartar, A., & Lazdunski, M. (1991) *Proc. Natl. Acad. Sci. U.S.A. 88*, 2437−2440.

Drevet, P., Lemaire, C., Gasparini, S., Zinn-Justin, S., Lajeunesse, E., Ducancel, F., Trémeau, O., Courson, M., Boulain, J.-C., & Ménez, A. (1997) *Protein Expression Purif.* (in press).

Ducancel, F., Mérienne, K., Fromen-Romano, C., Trémeau, O., Drevet, P., Pinkasfeld, S., Zinn-Justin, S., Boulain, J.-C., & Ménez, A. (1996) *J. Biol. Chem. 271*, 31345−31353.

Dufton, M. J., & Hider, R. C. (1991) in *Snake Toxins* (Harvey, A. L., Ed.) pp 259−302, Pergamon Press, New York.

Eaker, D., & Porath, J. (1967) P*roc. Plenary Sess., Int. Congr. Biochem., 7th, 1967 (1968) Col. VIII-3* (Abstract III), 499.

Endo, T., & Tamiya, N. (1991) in *Snake Toxins* (Harvey, A. L., Ed.) pp 165−222, Pergamon Press, New York.

Fraser, R. R., Boussard, G., Saunders, J. K., Lambert, J. B., & Mixan, C. E. (1971) *J. Am. Chem. Soc. 93*, 3822−3823.

Garcia de la Torre, J., & Bloomfield, V. A. (1981) *Q. Rev. Biophys. 14*, 81−139.

Grasberger, B. L., Gronenborn, A. M., & Clore, G. M. (1993) *J. Mol. Biol. 230*, 364−372.

Hansen, A. P., Petros, A. M., Meadows, R. P., & Fesik, S. W. (1994) *Biochemistry 33*, 15418−15424.

Kay, L. E., Nicholson, L. K., Delaglio, F., Bax, A., & Torchia, D. A. (1992) *J. Magn. Reson. 97*, 359−375.

Kolbe, H. V. J., Huber, A., Cordier, P., Rasmussen, U. B., Bouchon, B., Jacquinod, M., Vlasak, R., Délot, E. C., & Kreil, G. (1993) *J. Biol. Chem. 268*, 16458−16464.

Kopple, K. D., Wang, Y.-S., Cheng, A. G., & Bhandary, K. K. (1988) *J. Am. Chem. Soc. 110*, 4168−4176.

Kördel, J., Skelton, N. J., Akke, M., Palmer, A. G., & Chazin, W. (1992) *Biochemistry 31*, 4856−4866.

Le Du, M.-H., Marchot, P., Bougis, P. E., & Fontecilla-Camps, J. C. (1992) *J. Biol. Chem. 267*, 22122−22130.

Le Du, M.-H., Housset, D., Marchot, P., Bougis, P. E., Navaza, J., & Fontecilla-Camps, J. C. (1996) *Acta Crystallogr. D52*, 87−92.

Li, Y.-C., & Montelione, G. T. (1995) *Biochemistry 34*, 2408−2423.

Lipari, G., & Szabo, A. (1982) *J. Am. Chem. Soc. 104*, 4546−4559.

Marion, D., & Wüthrich, K., (1983) *Biochem. Biophys. Res. Commun. 113*, 967−974.

Marion, D., Ikura, M., Tschudin, R., & Bax, A. (1989) *J. Magn. Reson. 85*, 393−399.

McDowell, R. S., Dennis, M. S., Louie, A., Shuster, M., Mulkerrin, M. G., & Lazarus, R. A. (1992) *Biochemistry 31*, 4766−4772.

Miyazawa, T., Endo, F., Inagaki, K., Hayashi, K., & Tamiya, N. (1983) *Biopolymers 22*, 139−145.

Norwood, T. L., Boyd, J., Heritage, J. E., Soffe, N., & Campbell, I. (1990) *J. Magn. Reson. 87*, 488−501.

Otting, G., & Wüthrich, K. (1988) *J. Magn. Reson. 76*, 569−574.

Palmer, A. G., Rance, M., & Wright, P. E. (1991) *J. Am. Chem. Soc. 113*, 4371−4380.

Peng, J. W., & Wagner, G. (1992) *J. Magn. Reson. 98*, 308−332.

Pillet, L., Trémeau, O., Ducancel, F., Drevet, P., Zinn-Justin, S., Pinkasfeld, S., Boulain, J.-C., & Ménez, A. (1993) *J. Biol. Chem. 268*, 909−916.

Piotto, M., Saudek, V., & Sklenar, V. (1992) *J. Biomol. NMR 2*, 661−665.

Ploug, M., & Ellis, V. (1994) *FEBS Lett. 349*, 163−168.

Powers, R., Clore, G. M., Garret, D. S., & Gronenborn, A. M. (1993) *J. Magn. Reson. B101*, 325−327.

Press, W. H., Flannery, B. P., Teukolsky, S. A., & Vetterling, W. T. (1988) *Numerical Recipes in Fortran. The Art of Scientific Programming*, Cambridge University Press, Cambridge.
Redfield, C., Boyd, J., Smith, L. J., Smith, R. A. G., & Dobson, C. M. (1992) *Biochemistry 31*, 10431−10437.
Rodriguez-Ithurralde, D., Silveira, L., Barbeito, L., & Dajas, F. (1983) *Neurochem. Int. 5*, 267−274.
Schurr, J. M., Babcock, H. P., & Fujimoto, B. S. (1994) *J. Magn. Reson. B105*, 211−224.
Shaka, A. J., Keeler, J., & Freeman, R. (1983) *J. Magn. Reson. 53*, 313−340.
Sklenar, V., Torchia, D., & Bax, A. (1987) *J. Magn. Reson. 73*, 375−379.
Stone, M. J., Fairbrother, W. J., Palmer, A. G., Reizer, J., Saier, M. H., & Wright, P. E. (1992) *Biochemistry 31*, 4394−4406.
Sugita, Y., Nakano, Y., & Tomita, M. (1988) *J. Biochem. 104*, 633−637.
Szyperski, T., Luginbühl, P., Otting, G., Güntert, P., & Wüthrich, K. (1993) *J. Biomol. NMR 3*, 151−164.
Tjandra, N., Feller, S. E., Pastor, R. W., & Bax, A. (1995) *J. Am. Chem. Soc. 117*, 12562−12566.
Tjandra, N., Wingfield, P., Stahl, S., & Bax, A. (1996) *J. Biomol. NMR 8*, 273−284.
Trémeau, O., Lemaire, C. Drevet, P., Pinkasfeld, S., Ducancel, F., Boulain, J.-C., & Ménez, A. (1995) *J. Biol. Chem. 270*, 9362−9369.
Venable, R. M., & Pastor, R. W. (1988) *Biopolymers 27*, 1001−1014.
Woessner, D. E. (1962) *J. Chem. Phys. 3*, 647−654.
Zinn-Justin, S., Roumestand, C., Gilquin, B., Bontems, F., Ménez, A., & Toma, F. (1992) *Biochemistry 31*, 11335−11347.
Zinn-Justin, S., Roumestand, C., Drevet, P., Ménez, A., & Toma, F. (1993) *Biochemistry 32*, 6884−6891.
Zinn-Justin, S., Pillet, L., Ducancel, F., Thomas, A., Smith, J. C., Boulain, J.-C., & Ménez, A. (1994) *Protein Eng. 7*, 917−923.
Zinn-Justin, S., Guenneugues, M., Drakopoulou, E., Gilquin, B., Vita, C., & Ménez, A. (1996) *Biochemistry 35*, 8535−8543.
Zinn-Justin, S., Berthault, P., Guenneugues, M., & Desvaux, H. (1997) *J. Biomol. NMR* (in press).

BI971293K